Characterization of Transition Edge Sensors for the Millimeter Bolometer Array Camera on the Atacama Cosmology Telescope

Y. Zhao[a], C. Allen[b], M. Amiri[c], J. W. Appel[a], E. S. Battistelli[i,c], B. Burger[c], J. A. Chervenak[b], A. J. Dahlen[a], S. Denny[a], M. J. Devlin[d], S. R. Dicker[d], W. B. Doriese[e], R. Dünner[j,a], T. Essinger-Hileman[a], R. P. Fisher[a], J. W. Fowler[a], M. Halpern[c], G. C. Hilton[e], A. D. Hincks[a], K. D. Irwin[e], N. Jarosik[a], J. Klein[d], J. M. Lau[f], T. A. Marriage[g], K. L. Martocci[h], S. H. Moseley[b], M. D. Niemack[a], L. Page[a], L. P. Parker[a], A. Sederberg[a], S. T. Staggs[a], O. R. Stryzak[a], D. S. Swetz[d], E. R. Switzer[a], R. J. Thornton[d], E. J. Wollack[b]

[a]Dept. of Physics, Jadwin Hall, Princeton University, Princeton, NJ 08544, USA;
[b]Code 665, NASA Goddard Space Flight Center, Greenbelt, MD 20771, USA;
[c]Dept. of Physics and Astronomy, University of British Columbia, Vancouver, BC V6T 1Z1, Canada;
[d]Dept. of Physics and Astronomy, University of Pennsylvania, 209 South 33rd Street, Philadelphia, PA 19104, USA;
[e]National Institute of Standards and Technology, 325 Broadway, Boulder, CO 80305, USA;
[f]Dept. of Physics, Stanford University, 382 Via Pueblo Mall, Stanford, CA 94305, USA;
[g]Dept. of Astrophysical Sciences, Peyton Hall, Princeton University, Princeton, NJ 08544, USA;
[h]Dept. of Physics, City University of New York, 365 5th Avenue, Suite 6412, New York, NY 10016, USA;
[i]Dept. of Physics, University of Rome "La Sapienza", Piazzale Aldo Moro 5, I-00185 Rome, Italy;
[j]Dept. de Astronomía y Astrofísica, Facultad de Física, Pontificia Universidad Católica de Chile, Casilla 306, Santiago 22, Chile

ABSTRACT

The Atacama Cosmology Telescope (ACT) aims to measure the Cosmic Microwave Background (CMB) temperature anisotropies on arcminute scales. The primary receiver for ACT is the Millimeter Bolometer Array Camera (MBAC). The MBAC is comprised of three $32{\times}32$ transition edge sensor (TES) bolometer arrays, each observing the sky with an independent set of band-defining filters. The MBAC arrays will be the largest pop-up detector arrays fielded, and among the largest TES arrays built. Prior to its assembly into an array and installation into the MBAC, a column of 32 bolometers is tested at ~ 0.4 K in a quick-turn-around dip probe. In this paper we describe the properties of the ACT bolometers as revealed by data from those tests, emphasizing a characterization that accounts for both the complex impedance and the noise as a function of frequency.

Keywords: Transition edge sensor, detector, bolometer, array, complex impedance, noise, cosmology, CMB

1. INTRODUCTION

The Atacama Cosmology Telescope is a 6-meter off-axis Gregorian telescope for measuring the cosmic microwave background at arcminute resolutions.[1] The ACT project will produce high-resolution millimeter-wave maps of the sky, which can be analyzed to provide measurements of the cosmic microwave background angular power spectrum

Send correspondence to yuezhao@princeton.edu (Yue Zhao)

at large multipoles to augment the extant data[2–5] to improve estimation of such cosmological parameters as the scalar spectral index and its running, the density of baryons, and the scalar-to-tensor ratio.[6,7] When combined with X-ray and optical observations, the millimeter-wave maps will help to determine the equation of state of dark energy, probe the neutrino masses, constrain the time of the formation of the first stars, and reveal details of the growth of gravitationally bound structures in the universe.[8]

The primary receiver for ACT, the Millimeter Bolometer Array Camera, comprises three TES bolometer arrays centered at 145 GHz, 220 GHz, and 280 GHz respectively.[9] These three bands span the null of the Sunyaev-Zel'dovich Effect (SZE),[10] allowing separation of the primary CMB fluctuations from the SZE, and generation of an unbiased galaxy cluster catalog. Each of the three MBAC arrays consists of 32 column assemblies each containing 32 TES bolometers. The MBAC started observations in 2007 with the first array at 145 GHz.[11] The second array at 220 GHz has been completed, and the assembly of the third array at 280 GHz is near completion. Fig. 1 shows a picture of the 220 GHz MBAC bolometer array.
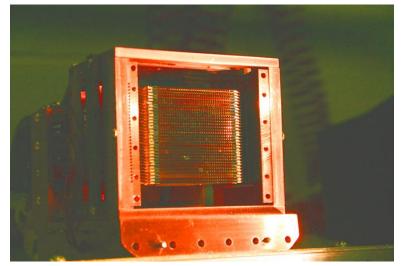

Figure 1. The 220 GHz 32×32 TES bolometer array of the MBAC after the completion of its assembly. The 32 column assemblies, stacked horizontally, sit in a copper mount. The total height of the 32 column assemblies is slightly larger than their width due to the vertical spacing of 170 μm between the two adjacent column assemblies.

Four separate silicon chips are mounted on a silicon circuit board for each column assembly: a TES bolometer chip, a shunt resistor chip with typical resistances of ~ 0.7 mΩ to voltage bias the TES, an inductor chip to bandlimit the TES response, and a multiplexing chip based on superconducting quantum interference devices (SQUIDs). The inductor chips and the multiplexing chips[12] were developed at NIST. ACT TES bolometers are pop-up devices[13,14] fabricated in the NASA Goddard Detector Development Laboratory. The shunt chips (also from Goddard) and the multiplexing chips are screened in a 4K dip probe, enabling us to select the best components for the column assemblies.

To evaluate the functionality and sensitivity of the detectors, each column assembly is tested in a cryostat called the Super Rapid Dip Probe (SRDP) prior to assembly into an array and installation into the MBAC. The SRDP measurements are made in the dark, with negligible photon power reaching the bolometers. In addition to obtaining essential TES parameters such as current-voltage (I-V) characteristics, saturation powers, and noise, on a subset of TES bolometers we also perform complex impedance measurements.

This is one of a series of papers[15–19] in these proceedings which describe technical aspects of ACT: the telescope, the cryogenic camera, the data acquisition, the optical characterization, and the coordination of ACT systems. In this paper we describe the characterization of the ACT bolometers with the SRDP data. We focus on modeling results based on the complex impedance and noise data.

2. MODELING OF ACT TES BOLOMETERS

A thermal detector may be modeled as a single lumped heat capacity C connected to a heat bath through a weak thermal link of conductance G,[20–22] as shown by Fig. 2(a). In this simple, or ideal, bolometer model the complex impedance and noise properties of a bolometer have been described by a number of authors.[23–27] Here we take note that in the small-signal limit, the complex impedance of a simple bolometer traces a semicircle in the complex plane as a function of frequency. In this model, for a typical voltage-biased TES bolometer with strong electrothermal feedback, the current noise at low frequency is dominated by random energy flow between the bolometer and the heat bath (also referred to as phonon noise), and there is a contribution at high frequency from Johnson noise.[28, 29]
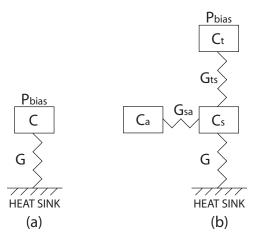

Figure 2. Thermal models of a TES bolometer. The simple model is shown on the left, and the extended model used to describe the ACT bolometers (whose complex impedance is described by Eq. (1)) is shown on the right. The parameters are defined in the text.

The above model can be extended to more complicated bolometers. In particular, the ACT bolometers exhibit behavior in complex impedance and noise that cannot be explained by the simple TES model, as shown by the measured complex impedance and noise data in Fig. 3 and Fig. 4. Each ACT bolometer has a 75 μm $\times$ 75 μm thin-film MoAu bilayer deposited on a 1 mm square of 1 μm thick silicon substrate. The MoAu bilayer is tuned to have a critical temperature around 0.5 K and a typical normal resistance between 20 and 30 mΩ. The silicon substrate is implanted with ions to absorb radiation power. Each bolometer is heat sunk through four legs made from the 1 μm thick silicon substrate. We present data below for a bolometer with a leg width of 13 μm. The three arrays for ACT have different saturation power and noise requirements, thus ACT uses bolometers with a variety of leg widths, from 5 to 20 μm. A Mo-Nb-Mo superconducting trilayer comprises the wiring to each TES. The silicon legs and the wiring of each TES are folded into a plane perpendicular to the absorber area (hence the name "pop-up detector").

We propose a thermal model for the ACT bolometers. This thermal model, which is depicted in Fig. 2(b), includes the TES MoAu bilayer heat capacity C_t at temperature T_t, the combined silicon substrate and ion implant heat capacity C_s at temperature T_s, a stray heat capacity C_a at temperature T_a, and the heat sink at temperature T_b. These components are connected by thermal links of different conductances as shown. The inclusion of the stray heat capacity C_a greatly improves the fit of the model to the data, as Fig. 3 shows. An attempt to assign an appropriate physical interpretation to the stray heat capacity is given in the conclusion section.

For power P_{ij} flowing from element i to element j, we consider the form

$$P_{ij} \;\; = \;\; K_{ij}\left(T_i^{n_{ij}} - T_j^{n_{ij}}\right),$$

where T_i and T_j are the temperatures of the elements i and j respectively and K_{ij} and n_{ij} are constants. The elements to be considered include the TES bilayer t, the silicon substrate (with implant) s, the stray heat capacity
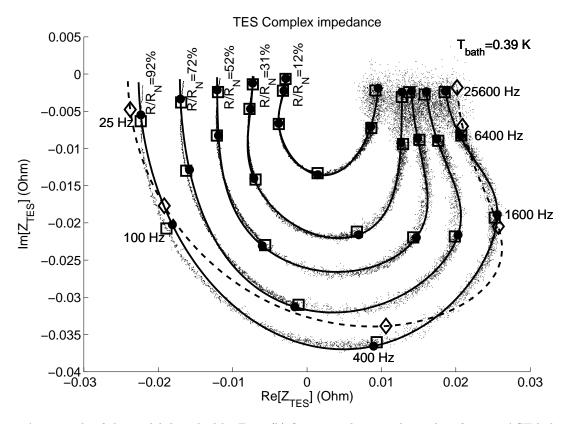
Figure 3. An example of the model described by Fig. 2(b) fit to complex impedance data from an ACT bolometer. The complex impedance data (dots) were taken at five TES operating resistances at a bath temperature of approximately 0.39 K. For each TES operating resistance, each dot represents the complex impedance at a different frequency. The model predictions (solid curves) use the global fit parameters listed in Table 1 at this bath temperature. The operating resistance for each of the five curves is printed at the top. We choose six representative frequencies and label them by solid circles on each of the model prediction curves; the values of these six frequencies are shown on the prediction curve for the highest operating resistance. The corresponding frequencies for the data are labeled by empty squares. The best global fit using a model described by Fig. 2(b) without the stray heat capacity (dashed curve with frequency evolution labeled by empty diamonds) is also shown for the highest operating resistance. The noise data of this ACT bolometer at the same bath temperature is shown in Fig. 4.

a, and the thermal bath b. We furthermore define the associated thermal conductances as

$$G_{\mathrm{ij}}^{\mathrm{i}} = \frac{\partial}{\partial T_{\mathrm{i}}} P_{\mathrm{ij}} = n_{\mathrm{ij}} K_{\mathrm{ij}} T_{\mathrm{i}}^{n_{\mathrm{ij}}-1},$$

$$G_{\mathrm{ij}}^{\mathrm{j}} = -\frac{\partial}{\partial T_{\mathrm{j}}} P_{\mathrm{ij}} = n_{\mathrm{ij}} K_{\mathrm{ij}} T_{\mathrm{j}}^{n_{\mathrm{ij}}-1}.$$

We assume that the equilibrium temperatures of the substrate and the stray heat capacity are equal, as in the case of zero net power flow between the substrate and the stray heat capacity. Because $G_{\mathrm{sa}}^{\mathrm{s}}$ and $G_{\mathrm{sa}}^{\mathrm{a}}$ are then equal when evaluated at the corresponding equilibrium temperatures, we ignore their superscripts and denote both of them by G_{sa}. In addition, because the bath temperature is fixed and thus $G_{\mathrm{sb}}^{\mathrm{b}}$ does not affect detector dynamics, we will write $G_{\mathrm{sb}}^{\mathrm{s}}$ as G for simplicity. We assume that the absorbed radiation power is zero.

Note that, if we map the TES MoAu bilayer to the TES electron system, the silicon substrate to the TES lattice system, and the stray heat capacity to the absorber, we get exactly the situation discussed in Galeazzi & Mc-Cammon 2003[26] for a bolometer with electron-lattice decoupling and lattice-absorber decoupling. We simply transform Eq. (110) in Galeazzi & McCammon 2003 as the Z_{TES} in our model:

$$\frac{Z_{\text{TES}}(\omega)}{R(\beta+1)} = \frac{\left[\left(G+G_{\text{ts}}^{\text{s}}+i\omega C_{\text{s}}\right)\left(1+i\omega\tau_{\text{a}}\right)+i\omega C_{\text{a}}\right]\left(G_{\text{ts}}^{\text{t}}+i\omega C_{\text{t}}+\dfrac{P\alpha}{T_{\text{t}}(\beta+1)}\right)-G_{\text{ts}}^{\text{t}}G_{\text{ts}}^{\text{s}}(1+i\omega\tau_{\text{a}})}{\left[\left(G+G_{\text{ts}}^{\text{s}}+i\omega C_{\text{s}}\right)\left(1+i\omega\tau_{\text{a}}\right)+i\omega C_{\text{a}}\right]\left(G_{\text{ts}}^{\text{t}}+i\omega C_{\text{t}}-\dfrac{P\alpha}{T_{\text{t}}}\right)-G_{\text{ts}}^{\text{t}}G_{\text{ts}}^{\text{s}}(1+i\omega\tau_{\text{a}})}, \quad (1)$$

where P is the bias power dissipated in the TES bilayer, $R = R(T_{\text{t}}, I)$ is the TES operating resistance, I is the current through the TES, $\tau_{\text{a}} = C_{\text{a}}/G_{\text{sa}}$ is the stray heat capacity time constant, and α, β are logarithmic derivatives:

$$\alpha = \frac{T_{\text{t}}}{R}\left(\frac{\partial R}{\partial T_{\text{t}}}\right), \text{ and } \beta = \frac{I}{R}\left(\frac{\partial R}{\partial I}\right).$$

3. EXPERIMENTS AND ANALYSIS

The SRDP is a ^{3}He dip probe refrigeration system to cool the TES thermal bath of a single column assembly from room temperature to ~ 0.4 K in three hours.[30] We use the SRDP to collect data for each of the approximately 100 columns needed for the three ACT arrays.

For each bolometer on a column assembly, we acquire SQUID V-ϕ curves to evaluate the multiplexing chip's performance, TES I-V curve to determine TES operating current, resistance and bias power as a function of applied TES bias voltage, TES noise spectra at multiple operating resistances, and noise spectrum when the TES is superconducting; this last measurement is used to extract the shunt resistance and the inductance in the TES loop from the observed Johnson noise level and its lowpassed filter response.[31] We also measure the TES critical temperature. For a subset of TES bolometers, we measure their I-V curves at multiple bath temperatures to obtain the parameters K_{sb}, n_{sb} and T_{t}, assuming K_{ts} is large so that $T_{\text{t}} \approx T_{\text{s}}$. For some of these TES bolometers, we also measure the TES transfer functions, complex impedances and noise spectra at different operating resistances and different bath temperatures. We use an HP 35670A spectrum analyzer to collect TES transfer functions, complex impedances and noise spectra.

We fit the model described by Fig. 2(b) to the complex impedance data, and compares the noise data to the predictions derived from the parameters extracted from the complex impedance fit. Following Lindeman *et al* 2007,[32] we construct a Thevenin equivalent circuit to extract the TES complex impedance. The free parameters in the fit of the model to the impedance data are α, β, C_{t}, C_{s}, K_{ts}, C_{a} and K_{sa}. In a global fit, we allow α, β, C_{t} to vary at different TES operating resistances and bath temperatures, while keeping C_{s}, K_{ts}, C_{a}, K_{sa} fixed. We assume that phonon transfer is the main heat transfer mechanism among the different components in the thermal circuit. We also fix $n_{\text{ts}} = 4$ and $n_{\text{sa}} = 4$, as in the case where phonons make no collisions over the connecting path between the two corresponding bodies.[33] When evaluating Eq. (1) during the fit, we calculate T_{s}, G_{ts}^{t}, G_{ts}^{s} from T_{t}, K_{ts}, n_{ts}, P_{ts}; G_{sa} from T_{s}, K_{sa}, n_{sa}; and G from T_{s}, K_{sb}, n_{sb}. If we choose n_{ts} and n_{sa} differently, K_{ts} and K_{sa} will change accordingly to keep G_{ts}^{t}, G_{ts}^{s}, G_{sa}, T_{s}, and hence G, approximately unchanged, while α, β, C_{t}, C_{s}, C_{a} will also largely remain fixed. The thermal conductances G_{ts}^{t}, G_{ts}^{s}, G_{sa}, G and the parameters α, β, C_{t}, C_{s}, C_{a} enter the calculation of complex impedance directly. Therefore the complex impedance fit is not sensitive to this particular choice of n_{ts} and n_{sa}. The extracted K_{ts} is much larger than K_{sb}. Hence T_{s} is close to T_{t}. Because of the robustness of the thermal conductance calculations described above and the small differences among T_{t}, T_{s} and T_{a}, our noise calculation is also insensitive to this particular choice of n_{ts} and n_{sa}.[34] Changing the heat transfer mechanism between the TES bilayer and the silicon substrate or between the silicon substrate and the stray heat capacity to electron-phonon decoupling only slightly changes the noise calculation.[35]

4. RESULTS AND DISCUSSIONS

Table 1 summarizes the parameters extracted from the fit of the model described by Fig. 2(b) to complex impedance data taken at different TES operating resistances at two different bath temperatures on a particular ACT bolometer. Although we describe here the model fit on just one ACT bolometer, we have obtained qualitatively similar results on eight ACT bolometers in three column assemblies for which sufficient complex

R/R_n, T_bath (K)	12%, 0.317	31%, 0.317	52%, 0.318	72%, 0.318	93%, 0.318
α	176 (169)	136 (124)	113 (109)	95 (95)	67 (68)
β	2.47 (2.40)	0.80 (0.78)	0.30 (0.29)	0.09 (0.09)	-0.01 (0.00)
C_t(pJ/K)	0.33 (0.30)	0.33 (0.29)	0.33 (0.31)	0.33 (0.32)	0.32 (0.33)
R/R_n, T_bath (K)	12%, 0.393	31%, 0.394	52%, 0.394	72%, 0.394	92%, 0.394
α	236 (188)	178 (172)	132 (139)	106 (111)	81 (82)
β	2.95 (2.90)	0.97 (0.95)	0.31 (0.31)	0.07 (0.08)	-0.03 (-0.03)
C_t(pJ/K)	0.32 (0.25)	0.32 (0.30)	0.33 (0.34)	0.32 (0.35)	0.31 (0.33)
C_s(pJ/K)	1.30 (1.22± 0.17)				
K_ts(nW/K^4)	15.5 (15.5± 1.0)				
C_a(pJ/K)	0.96 (0.93± 0.06)				
K_sa(nW/K^4)	4.2 (4.7± 1.0)				

Table 1. An instance of the extracted parameters from fitting the model described by Fig. 2(b) to the complex impedance data of an ACT bolometer. The first four rows in this table are for a bath temperature of approximately 0.32 K, and the next four rows are for a bath temperature of approximately 0.39 K. The complex impedance data with model fits and the noise data with predictions of this ACT bolometer at the bath temperature of 0.39 K are shown in Fig. 3 and Fig. 4. As described in the text, results from other ACT bolometers are qualitatively similar. For each fit parameter, the table gives two estimates to illustrate robustness. The first comes from the global fit described in the text. The parenthetical estimate comes from refitting all the parameters at each specified bath temperature and TES operating resistance combination. For the parenthetical estimates of C_s, K_ts, C_a and K_sa, we list their averages and standard deviations across the two bath temperatures and all TES operating resistances, instead of giving their values at each individual bath temperature and operating resistance combination. The extracted parameters in this table have not been verified by independent measurements and can be far from their expectations, as discussed in the text.

impedance and noise data have been acquired. Fig. 3 shows the complex impedance data with its fit at one of these two bath temperatures, and Fig. 4 compares the noise data to the predictions derived from the parameters extracted from the complex impedance fit at the same bath temperature.

To estimate the error on the extracted parameters, we also fit the model to complex impedance data at each combination of TES operating resistance and bath temperature, and compare the resulting parameters to those from the global fit. The parameters obtained from these two different methods agree to approximately 10% in most cases, as indicated by Table 1.

The complex impedance fits show reasonable agreement with the data from 10 Hz to 10 kHz, and the noise predictions are in general accurate in the same frequency band. The random energy flow between the silicon substrate and the heat bath is insufficient to account for all the noise in the frequency band of interest to ACT, from ~ 1 Hz to ~ 100 Hz.[36] At present, the detector model predicts that the excess noise in this frequency band is due to random energy flow between the TES bilayer and the silicon substrate, as well as between the silicon substrate and the stray heat capacity.

Several of the extracted parameters are far from their expectations, suggesting that the current physical interpretation of the model may be flawed. For instance, the fit results in an extracted thermal conductance G_ts^t between the TES bilayer and the silicon substrate of approximately 6 nW/K. This value is at least an order of magnitude smaller than the expected combination of the TES electron-lattice decoupling and the Kapitza resistance between the TES lattice system and the silicon substrate.[37] However, this relatively small G_ts^t is necessary to explain the peak in the noise data at ~ 2 kHz. The discrepancy between the extracted thermal conductance G_ts^t and the calculated one indicates that the TES bilayer-silicon substrate thermal coupling in the ACT bolometers is not as tight as we expected, or that the decoupling suggested by the model is not between the TES bilayer and the silicon substrate as in the current interpretation, among other possibilities.

We also note that the sum of the silicon substrate and the stray heat capacity extracted from the complex
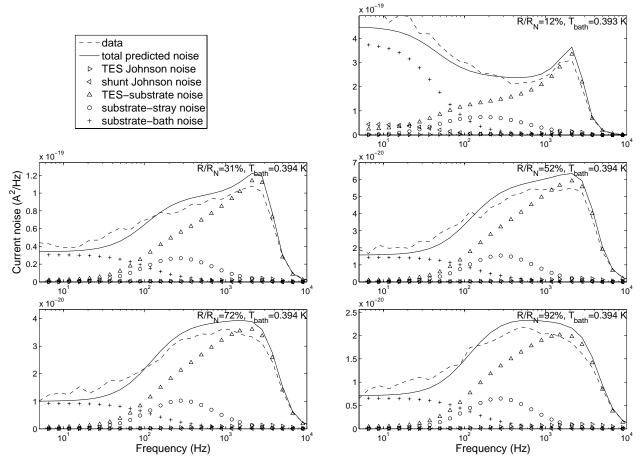
Figure 4. Comparison of noise data to predictions derived from the parameters extracted from the complex impedance fit at a bath temperature of approximately 0.39 K for the bolometer described in Table 1 and Fig. 3. The decomposition of the predicted noise into different contributors is also shown. In particular, "TES-substrate noise", "substrate-stray noise" and "substrate-bath noise" represent the noise contributed by random power flows between the corresponding components in the thermal circuit described by Fig. 2(b). The noise data shown have been smoothed.

impedance fit, which is around 2 pJ/K, is larger than the expected heat capacity of approximately 1 pJ/K of the silicon substrate with ion implant. In addition, the extracted heat capacity of the TES bilayer is approximately two to three times higher than the current estimate. We have postulated several candidates for the origin of the additional heat capacity unaccounted for by our calculation, such as the silicon legs or the TES wiring, but at present we have no data to support these ideas.

We have also implemented other models for the ACT bolometers, such as thermal circuits with only two separate heat capacities, and another thermal circuit with three heat capacities, one of which is a heat capacity on the silicon legs instead of a stray heat capacity connected to the silicon substrate. The two-heat-capacity models do not fit the complex impedance data well, independent of which heat capacity we designate as the TES bilayer. One example of a complex impedance fit of a two-heat-capacity model described by Fig. 2(b) without the stray heat capacity is shown in Fig. 3. The fits of the model to complex impedance data and the total noise predictions in the the heat-capacity-on-the-leg case are almost identical to those obtained in the model described by Fig. 2(b).

5. CONCLUSIONS AND PLANS

We have described a model for the ACT bolometers. This model explains our observed TES complex impedance and noise behavior reasonably well. However, several extracted parameters from the model fit are far from expectations, suggesting that the real physical interpretation of the model may be missing. We plan to carry out several concrete experiments to seek a better understanding of the model. For example, we plan to test TES bolometers with different heat capacity configurations, such as a TES bolometer with a silicon substrate not implanted with ions (which should result in significantly reduced heat capacity of the silicon substrate). Examining what modifications these configurations introduce to the parameters extracted from the complex impedance fit could help to determine the origin of the stray heat capacity and to break the degeneracy between the model described by Fig. 2(b) and the alternate heat-capacity-on-the-leg model described above. We also plan to test a TES bolometer whose silicon substrate is directly heat sunk to the heat bath (instead of through the silicon legs) to extract the thermal conductance between the TES bilayer and the silicon substrate and to explore the cause of the unexpectedly small value of this thermal conductance in the current model fit. Several of the bolometers for which we have made fits to complex impedance data are now in the MBAC. We plan to measure their time constants – their current response to changing voltage bias or optical power as a function of frequency. Because our thermal model predicts different time constants for the different components in the TES thermal circuit (in particular the TES bilayer in which bias power is dissipated and the implant layer in which photon power is absorbed), comparing the predicted time constants to the measured ones could help us appropriately interpret the TES model. The insights we gain through a sound TES model may inform future TES bolometer designs.

ACKNOWLEDGMENTS

REFERENCES

[1] Fowler, J. W., "The Atacama Cosmology Telescope Project," in [*Millimeter and Submillimeter Detectors for Astronomy II*], Zmuidzinas, J., Holland, W. S., and Withington, S., eds., *Proc. SPIE* **5498**, 1–10 (2004).

[2] Hinshaw, G., Weiland, J. L., Hill, R. S., Odegard, N., Larson, D., Bennett, C. L., Dunkley, J., Gold, B., Greason, M. R., Jarosik, N., Komatsu, E., Nolta, M. R., Page, L., Spergel, D. N., Wollack, E., Halpern, M., Kogut, A., Limon, M., Meyer, S. S., Tucker, G. S., and Wright, E. L., "Five-year Wilkinson Microwave Anisotropy Probe (WMAP) observations: Data processing, sky maps, and basic results," *ArXiv e-prints* **803** (2008).

[3] Mason, B. S., Pearson, T. J., Readhead, A. C. S., Shepherd, M. C., Sievers, J., Udomprasert, P. S., Cartwright, J. K., Farmer, A. J., Padin, S., Myers, S. T., Bond, J. R., Contaldi, C. R., Pen, U., Prunet, S., Pogosyan, D., Carlstrom, J. E., Kovac, J., Leitch, E. M., Pryke, C., Halverson, N. W., Holzapfel, W. L., Altamirano, P., Bronfman, L., Casassus, S., May, J., and Joy, M., "The anisotropy of the microwave background to $l = 3500$: deep field observations with the Cosmic Background Imager," *Astrophys. J.* **591**, 540–555 (2003).

[4] Reichardt, C., Ade, P. A. R., Bock, J. J., Bond, J. R., Brevik, J. A., Contaldi, C. R., Daub, M. D., Dempsey, J. T., Goldstein, J. H., Holzapfel, W. L., Kuo, C. L., Lange, A. E., Lueker, M., Newcomb, M., Peterson, J. B., Ruhl, J., Runyan, M. C., and Staniszewski, Z., "High resolution CMB power spectrum from the complete ACBAR data set," *ArXiv e-prints* **801** (2008).

[5] Sayers, J., Golwala, S. R., Rossinot, P., Ade, P. A. R., Aguirre, J. E., Bock, J. J., Edgington, S. F., Glenn, J., Goldin, A., Haig, D., Lange, A. E., Laurent, G. T., Mauskopf, P. D., and Nguyen, H. T., "A search for cosmic microwave background anisotropies on arcminute scales with Bolocam," *ArXiv e-prints* **805** (2008).

[6] Komatsu, E., Dunkley, J., Nolta, M. R., Bennett, C. L., Gold, B., Hinshaw, G., Jarosik, N., Larson, D., Limon, M., Page, L., Spergel, D. N., Halpern, M., Hill, R. S., Kogut, A., Meyer, S. S., Tucker, G. S., Weiland, J. L., Wollack, E., and Wright, E. L., "Five-year Wilkinson Microwave Anisotropy Probe (WMAP) observations: Cosmological interpretation," *ArXiv e-prints* **803** (2008).

[7] Ruhl, J. E., Ade, P. A. R., Carlstrom, J. E., Cho, H. M., Crawford, T., Dobbs, M., Greer, C. H., Halverson, N. W., Holzapfel, W. L., Lanting, T. M., Lee, A. T., Leitch, E. M., Leong, J., Lu, W., Lueker, M., Mehl, J., Meyer, S. S., Mohr, J. J., Padin, S., Plagge, T., Pryke, C., Runyan, M. C., Schwan, D., Sharp, M. K., Spieler, H., Staniszewski, Z., and Stark, A. A., "The South Pole Telescope," in [*Millimeter and Submillimeter Detectors for Astronomy II*], Zmuidzinaas, J., Holland, W. S., and Withington, S., eds., *Proc. SPIE* **5498**, 11–29 (2004).

[8] Kosowsky, A., "The Atacama Cosmology Telescope," *New Astron. Rev.* **47**, 939–943 (2003).

[9] Fowler, J. W., Niemack, M. D., Dicker, S. R., Aboobaker, A. M., Ade, P. A. R., Battistelli, E. S., Devlin, M. J., Fisher, R. P., Halpern, M., Hargrave, P. C., Hincks, A. D., Kaul, M., Klein, J., Lau, J. M., Limon, M., Marriage, T. A., Mauskopf, P. D., Page, L., Staggs, S. T., Swetz, D. S., Switzer, E. R., Thornton, R. J., and Tucker, C. E., "Optical design of the Atacama Cosmology Telescope and the Millimeter Bolometric Array Camera," *Appl. Opt.* **46**(17), 3444–3454 (2007).

[10] Carlstrom, J. E., Holder, G. P., and Reese, E. D., "Cosmology with the Sunyaev-Zel'dovich Effect," *Annu. Rev. Astron. Astrophys.* **40**, 643–680 (2002).

[11] Niemack, M. D., Zhao, Y., Wollack, E., Thornton, R., Switzer, E. R., Swetz, D. S., Staggs, S. T., Page, L., Stryzak, O., Moseley, H., Marriage, T. A., Limon, M., Lau, J. M., Klein, J., Kaul, M., Jarosik, N., Irwin, K. D., Hincks, A. D., Hilton, G. C., Halpern, M., Fowler, J. W., Fisher, R. P., Dünner, R., Doriese, W. B., Dicker, S. R., Devlin, M. J., Chervenak, J., Burger, B., Battistelli, E. S., Appel, J., Amiri, M., Allen, C., and Aboobaker, A. M., "A kilopixel array of TES bolometers for ACT: Development, testing, and first light," *J. Low Temp. Phys.* **151**(3-4), 690–696 (2008).

[12] Doriese, W. B., Beall, J. A., Duncan, W. D., Ferreira, L., Hilton, G. C., Irwin, K. D., Reintsema, C. D., Ullom, J. N., Vale, L. R., and Xu, Y., "Progress toward kilopixel arrays: 3.8 eV microcalorimeter resolution in 8-channel SQUID multiplexer," *Nuc. Inst. & Meth. in Phys. Res. A* **559**, 808–810 (2006).

[13] Benford, D. J., Staguhn, J. G., Stacey, G. J., Page, L. A., Moseley, S. H., Irwin, K. D., Chervenak, J. A., and Allen, C. A., "Design and fabrication of two-dimensional superconducting bolometer arrays," in [*Millimeter and Submillimeter Detectors for Astronomy II*], Zmuidzinas, J., Holland, W. S., and Withington, S., eds., *Proc. SPIE* **5498**, 647–658 (2004).

[14] Benford, D. J., Chervenak, J. A., Irwin, K. D., and Moseley, S. H., "Ultralow-background large-format bolometer arrays," in [*IR Space Telescopes and Instruments*], Mather, J. C., ed., *Proc. SPIE* **4850**, 944–953 (2003).

[15] Battistelli, E. S., Amiri, M., Burger, B., Devlin, M. J., Dicker, S. R., Doriese, W. B., Dünner, R., Fisher, R. P., Fowler, J. W., Halpern, M., Hasselfield, M., Hilton, G. C., Hincks, A. D., Irwin, K. D., Kaul, M., Klein, J., Knotek, S., Lau, J. M., Limon, M., Marriage, T. A., Niemack, M. D., Page, L., Reintsema, C. D., Staggs, S. T., Swetz, D. S., Switzer, E. R., Thornton, R. J., and Zhao, Y., "Automated SQUID tuning procedure for kilo-pixel arrays of TES bolometers on the Atacama Cosmology Telescope," *Also in these Proc. SPIE* .

[16] Hincks, A. D., Ade, P. A. R., Allen, C., Amiri, M., Appel, J. W., Battistelli, E. S., Burger, B., Chervenak, J. A., Dahlen, A. J., Denny, S., Devlin, M. J., Dicker, S. R., Doriese, W. B., Dünner, R., Essinger-Hileman, T., Fisher, R. P., Fowler, J. W., Halpern, M., Hargrave, P. C., Hasselfield, M., Hilton, G. C., Irwin, K. D., Jarosik, N., Kaul, M., Klein, J., Lau, J. M., Limon, M., Lupton, R. H., Marriage, T. A., Martocci, K. L., Mauskopf, P., Moseley, S. H., Netterfield, C. B., Niemack, M. D., Nolta, M. R., Page, L., Parker, L. P., Sederberg, A. J., Staggs, S. T., Stryzak, O. R., Swetz, D. S., Switzer, E. R., Thornton, R. J., Tucker, C., Wollack, E. J., and Zhao, Y., "The effects of the mechanical performance and alignment of the Atacama Cosmology Telescope on the sensitivity of microwave observations," *Also in these Proc. SPIE* .

[17] Swetz, D. S., Ade, P. A. R., Allen, C., Amiri, M., Appel, J. W., Battistelli, E. S., Burger, B., Chervenak, J. A., Dahlen, A. J., Das, S., Denny, S., Devlin, M. J., Dicker, S. R., Doriese, W. B., Dünner, R., Essinger-Hileman, T., Fisher, R. P., Fowler, J. W., Gao, X., Hajian, A., Halpern, M., Hargrave, P. C., Hasselfield, M., Hilton, G. C., Hincks, A. D., Irwin, K. D., Jarosik, N., Kaul, M., Klein, J., Knotek, S., Lau, J. M., Limon, M., Lupton, R. H., Marriage, T. A., Martocci, K. L., Mauskopf, P., Moseley, S. H., Netterfield, C. B., Niemack, M. D., Nolta, M. R., Page, L., Parker, L. P., Reid, B. A., Reintsema, C. D., Sederberg, A., Sehgal, N., Sievers, J. L., Spergel, D. N., Staggs, S. T., Stryzak, O. R., Switzer, E. R., Thornton, R. J., Tucker, C.,

Wollack, E. J., and Zhao, Y., "Instrument design and characterization of the Millimeter Bolometer Array Camera for the Atacama Cosmology Telescope," *Also in these Proc. SPIE* .

[18] Switzer, E. R., Allen, C., Amiri, M., Appel, J. W., Battistelli, E. S., Burger, B., Chervenak, J. A., Dahlen, A., Das, S., Devlin, M. J., Dicker, S. R., Doriese, W. B., Dünner, R., Essinger-Hileman, T., Fisher, R. P., Fowler, J. W., Gao, X., Halpern, M., Hasselfield, M., Hilton, G. C., Hincks, A. D., Irwin, K. D., Jarosik, N., Kaul, M., Knotek, S., Klein, J., Lau, J. M., Limon, M., Lupton, R. H., Marriage, T. A., Martocci, K., Moseley, H., Netterfield, B., Niemack, M. D., Nolta, M., Page, L., Parker, L. P., Reid, B., Reintsema, C. D., Sederberg, A., Sievers, J. L., Spergel, D., Staggs, S. T., Stryzak, O., Swetz, D. S., Thornton, R., Wollack, E., and Zhao, Y., "Systems and control software for the Atacama Cosmology Telescope," *Also in these Proc. SPIE* .

[19] Thornton, R. J., Ade, P. A. R., Allen, C., Amiri, M., Appel, J. W., Battistelli, E. S., Burger, B., Chervenak, J. A., Devlin, M. J., Dicker, S. R., Doriese, W. B., Essinger-Hileman, T., Fisher, R. P., Fowler, J. W., Halpern, M., Hargrave, P. C., Hasselfield, M., Hilton, G. C., Hincks, A. D., Irwin, K. D., Jarosik, N., Kaul, M., Klein, J., Lau, J. M., Limon, M., Marriage, T. A., Martocci, K., Mauskopf, P., Moseley, H., Niemack, M. D., Page, L., Parker, L. P., Reidel, J., Reintsema, C. D., Staggs, S. T., Stryzak, O. R., Swetz, D. S., Switzer, E. R., Tucker, C., Wollack, E. J., and Zhao, Y., "Opto-mechanical design and performance of a compact three-frequency camera for the MBAC receiver on the Atacama Cosmology Telescope," *Also in these Proc. SPIE* .

[20] Jones, R. C., "The ultimate sensitivity of radiation detectors," *J. Opt. Soc. Am.* **37**(11), 879–890 (1947).

[21] Low, F. J., "Low-temperature germanium bolometer," *J. Opt. Soc. Am.* **51**(11), 1300–1304 (1961).

[22] Mather, J. C., "Bolometer noise: nonequilibrium theory," *Appl. Opt.* **21**(6), 1125–1129 (1982).

[23] Mather, J. C., "Electrical self-calibration of nonideal bolometers," *Appl. Opt.* **23**(18), 3181–3183 (1984).

[24] Lindeman, M. A., Bandler, S., Brekosky, R. P., Chervenak, J. A., Figueroa-Feliciano, E., Finkbeiner, F. M., Li, M. J., and Kilbourne, C. A., "Impedance measurements and modeling of a transition-edge-sensor calorimeter," *Rev. Sci. Inst.* **75**(5), 1283–1289 (2004).

[25] Irwin, K. D. and Hilton, G. C., "Transition Edge Sensors," in [*Cryogenic Particle Detection*], Enss, C., ed., Springer-Verlag Berlin Heidelberg (2005).

[26] Galeazzi, M. and McCammon, D., "Microcalorimeter and bolometer model," *J. Appl. Phys.* **93**(8), 4856–4869 (2003).

[27] Figueroa-Feliciano, E., *Theory and development of position-sensitive quantum calorimeters*, PhD thesis, Stanford University (2001).

[28] Irwin, K. D., *Phonon-mediated particle detection using superconducting tungsten transition-edge sensors*, PhD thesis, Stanford University (1995).

[29] Lindeman, M. A., *Microcalorimetry and the transition-edge sensor*, PhD thesis, University of California at Davis (2000).

[30] Marriage, T. A., Chervenak, J. A., and Doriese, W. B., "Testing and assembly of the detectors for the Millimeter Bolometer Array Camera on ACT," *Nuc. Inst. & Meth. in Phys. Res. A* **559**, 551–553 (2006).

[31] Niemack, M. D., *Towards dark energy: design, development, and preliminary data from ACT*, PhD thesis, Princeton University (2008).

[32] Lindeman, M. A., Barger, K. A., Brandl, D. E., Crowder, S. G., Rocks, L., and McCammon, D., "Complex impedance measurements of calorimeters and bolometers: Correction for stray impedances," *Rev. Sci. Inst.* **78**, 043105 (2007).

[33] Boyle, W. S. and Rodgers, Jr., K. F., "Performance characteristics of a new low-temperature bolometer," *J. Opt. Soc. Am.* **49**(1), 66–69 (1959).

[34] McCammon, D., "Thermal equilibrium calorimeters – an introduction," in [*Cryogenic Particle Detection*], Enss, C., ed., Springer-Verlag Berlin Heidelberg (2005).

[35] Golwala, S. R., Jochum, J., and Sadoulet, B., "Noise considerations in low resistance NIS tunnel junctions," in [*Proceedings of the Seventh International Workshop on Low Temperature Detectors*], Cooper, S., ed., 56–59 (1997).

[36] Niemack, M. D., "Measuring two-millimeter radiation with a prototype multiplexed TES receiver for ACT," in [*Millimeter and Submillimeter Detectors and Instrumentation for Astronomy III*], Zmuidzinas, J., Holland, W. S., Withington, S., and Duncan, W. D., eds., *Proc. SPIE* **6275**, 62750C (2006).

[37] Chervenak, J. A. (2008). Personal communication.